Acta Geodyn. Geomater., Vol. 14, No. 3 (187), 297–304, 2017
DOI: 10.13168/AGG.2017.0012
journal homepage: https://www.irsm.cas.cz/acta

ORIGINAL PAPER

DOWNHOLE MICROSEISMIC MONITORING OF SHALE DEPOSITS: CASE STUDY FROM NORTHERN POLAND

Eryk ŚWIĘCH [1)]*, Paweł WANDYCZ [1)], Leo EISNER [2)], Andrzej PASTERNACKI [1)] and Tomasz MAĆKOWSKI [1)]

[1)] *AGH University of Science and Technology, Faculty of Geology, Geophysics and Environmental Protection, Department of Fossil Fuels, Al. Mickiewicza 30, 30–059 Kraków, Poland*
[2)] *Institute of Rock Structure and Mechanics, The Academy of Science of the Czech Republic, V Holešovičkách 41, 182 09 Praha 8, Czech Republic*

**Corresponding author's e-mail:* swiech.eryk@gmail.com

ARTICLE INFO

Article history:
Received 2 November 2016
Accepted 25 April 2017
Available online 11 May 2017

Keywords:
Polish shale gas
Downhole microseismic processing
Anisotropy
Microseismic events

ABSTRACT

Microseismic monitoring has become a standard technique to map the development of hydraulic fracturing. This study is a case study of a downhole monitoring of the hydraulic fracturing in a lateral well in Northern Poland.
The downhole monitoring array detected a large number of microseismic events indicating successful development of a hydraulic fracture. We show evidence that some stages interacted with the pre-existing natural fault system also mapped from surface active seismic imaging. The mapped hydraulic fracture shows a slight asymmetry of the developed hydraulic fractures. We show that the observed microseismicity is consistent with microseismicity usually observed in the North American shale gas stimulations.

INTRODUCTION

Unconventional shale oil and gas formations play an important role in worldwide resources these days. Low permeability of these formations requires hydraulic fracturing stimulations to allow the oil or the gas flow through the reservoir into production wells. Hydraulic fracturing, water injection, fluid extraction, and other reservoir activities usually result in brittle failure of the rocks with release of seismic energy, i.e. microseismicity (Duncan and Eisner, 2010). Location and characterization of these rock failures is the main purpose of a microseismic monitoring and this monitoring is used to optimize the shale stimulations. To correctly interpret the microseismicity we need to understand the location accuracy which is controlled by the monitoring network, the accuracy of arrival time picks, particle polarization, processing method and the velocity model. The proper calibration of the velocity model plays crucial role in case of reducing location uncertainty (e.g. Bardainne and Gaucher, 2010). This calibration usually involves seismic anisotropy of shale deposits (e.g., Grechka et al., 2011).

In this study, we describe a downhole microseismic monitoring from one of the first shale gas exploration experiment in north Poland. This site was characterized by Kowalski et al. (2014) using full – azimuth active seismic depth imaging and other geophysical datasets. They observed the target shale formation at the depth of 2800 m although the imaging results provided only limited accuracy probably due to high attenuation of the overburden. We analyze microseismic downhole dataset in the same region and compare the results with active seismic imaging. Although this stimulation was also monitored with a surface monitoring array, the array did not provide useful information and the surface monitoring is not discussed in this article.

Additional motivation for this analysis was to compare the induced microseismicity with the induced microseismicity in the North American plays where the shale gas is economically produced. Our results show that we observe similar development of microseismicity based on locations and similar change of source mechanisms of the induced microseismic events as reported by Stanek and Eisner (2013) and Grechka et al. (2011) in the North American shales.

SITE AND DATASET DESCRIPTION

The microseismic dataset was acquired during hydraulic fracturing of the Lower Silurian and Ordovician Formations in the Baltic Basin margin, Lubocino, North Poland. The area is situated in the western part of the Peri-Baltic Depression. The listostratigraphic profile of the area is represented by the Precambrian crystalline basement, and deposits of the Eocambrian, Cambrian, Ordovician, Silurian, Zechstein (Permian), Triassic, Jurassic, Cretaceous

Cite this article as: Święch E, Wandycz P, Eisner L, Pasternacki A, Maćkowski T: Downhole microseiseismic monitoring of shale deposits case staudy from Northern Poland. Acta Geodyn. Geomater., 14, No. 3 (187), 297–304, 2017.
DOI: 10.13168/AGG.2017.0012

and Cenozoic periods. The clastic series that fill this part of Peri-Baltic Depression creates two main complexes: one is Caledonia orogeny that encompasses deposits of the Cambrian to Silurian periods, second associated with Laramian phase, includes Permian to Cretaceous.

As shown in Figure 1, two wells were drilled at this site: one with a horizontal section (L2H) and one vertical (L1) well. The target interval is approximately at 2800 m true vertical depth sub sea (TVDSS) and mainly consists of fine grained siltstones with thickness of 30 m. The horizontal section of the stimulated L2H well is approximately 700 m long in the south-south-west direction. Distance between the vertical monitoring well (L1) and toe of the horizontal well (L2H) is exceeding 800 m. Hydraulic fracturing was carried out in 6 stages starting at the toe and progressing towards the heal of the L2H well. Eleven perforation shots were used in Stages 2 to 6 to connect the well with the reservoir, the first stage was connected through waterjet without using a perforations. The average distance between stages is approximately 100 m.

The monitoring array comprises of eleven three – components geophones with spacing 15 m between them spanning approximately 150 m. The array was deployed above the target interval with the lowest receiver at the depth of 2515 m, so there was no receiver at or below the fractured reservoir which increases the vertical uncertainties in microseismic event location. The non-linear grid search location algorithm is described in Eisner et al. (2010). Note, that the location uncertainty is influenced by particle polarization. It is well known (Rutledge and Phillips, 2003; Maxwell et al., 2010) that the vertical monitoring borehole in the horizontally stratified layer can constrain only distance and depth from the P- and S-wave arrival times. This information needs to be completed with back azimuth usually derived from P-wave polarization or S-wave polarization (Eisner et al., 2010).

The majority of recorded microseismic events in this dataset have very clear arrivals of the P- and S-waves, but due to the strong anisotropy of investigated geological interval, the S-wave arrivals are always splitted, which can be observed even for the perforation shots (Fig. 2). However, relatively strong P-wave arrivals allowed to determine back azimuths directly from the P-waves in this dataset.

MICROSEISMICITY PROCESSING

The observed shear wave splitting indicated we need to construct an anisotropic velocity model and calibrate the initial velocity model. We observed S-wave splitting into quasi SH and quasi SV waves. For this purpose sonic log, active seismic data and available perforation shots were used.

VELOCITY MODEL CALIBRATION

The initial 1D isotropic velocity model can be built using sonic logs (Warpinski et al., 2005) and then calibrated with check shots from the known locations (e.g., Maxwell et al., 2010).

In this study a simple layered 1D velocity model was built based on sonic logs (DTS and DTP) acquired in Lubocino – 1 well (these velocities were also calibrated by core measurements) (Fig. 3). Minimum thickness of layers was set to 40 m because observed seismic waves had the peak (Eisner et al., 2010) frequency at 100 Hz and P-wave minimum wavelength is approximately 40 m.

Figure 4a shows all available eleven perforation shots located in the initial isotropic velocity model. The map view reveals that the located shots do not differ significantly (within the estimated uncertainty of the location) from their true positions but they are located too shallow and there is a trend of the depth discrepancy with distance from the monitoring well.

Using a grid search we found a set of weak anisotropic parameters that allowed us to locate all perforation shots within the uncertainty of the location to their true position shown in Figure 4b. This VTI velocity model has effective anisotropic parameters $\eta = 0.07$ and $\gamma = 0.18$ (η and γ are defined by Grechka et al. (1999) for all layers of the velocity model. The VTI model removed the trend of locations in isotropic model while horizontal locations are still very good and we were able to locate perforation shots within the uncertainty to their true positions. Note that the back azimuth measured from the P-wave particle polarizations has constrained the locations of the perforations relatively well with a small scatter corresponding to several degrees. Based on observed polarizations of P-waves we have set the average uncertainty of the back azimuths to 7 degrees which is consistent with reported uncertainties in other case studies (e.g. Menanno et al., 2012). Additionally the arrival time pick uncertainty was set to 5 milliseconds which is the upper bound of the achieved travel time residuals.

The found VTI parameter η is similar to the value of 0.08 derived from the active seismic imaging of these layers (Smolarski et al., 2014).

MICROSEISMIC EVENTS LOCATIONS

The total number of detected and located microseismic events from all six stages is 844. To achieve the most reliable events positions the P- and S-wave arrivals were picked on peak amplitude (Rutledge and Phillips, 2003). We picked the SH-wave (East component) of the S-waves and used the SH-velocities to locate the microseismic events. To determine the back azimuth of the events we used only the P-wave arrivals.

The map view of the microseismic events located in the calibrated anisotropic velocity model is shown in Figure 5a. We observe asymmetric growth

around the treatment well with more events located to the east of the treatment well mostly for Stage 5 as discussed later. Similar asymmetry of the hydraulic fractures is commonly observed also in the North American datasets and can be explained by a pore-pressure gradient (e.g., Fischer et al., 2008). Stages 1 and 2 are slightly offset from the injection point (true locations of the perforations) but note that the offset is similar to the offset of the perforation of Stage 2. While this is certainly unfortunate the Stage 2 is located more than 4 spans of the monitoring array from the nearest receiver and the locations are simply very uncertain. We observe horizontal growth of the hydraulic fracture of approximately 150 m in east–west direction similar to distances observed in the North American datasets.

3D view (Fig. 5b) shows that the most of located seismicity stayed in the depth of the treatment well. Although the events are located slightly below the treatment well, the depth difference between the event locations and treatment well is within the uncertainty of the locations, especially for the further stages. Figure 5b also shows a group of events from Stage 4 and 5 located at shallower depth than the injection point which is consistent with reactivation of a fault. Events located at shallower depth occurred at the end of the stimulation. Those events have very similar waveforms to each other but do not differ significantly from rest of the recorded events. In the area of the study a conventional 3D seismic survey was carried out by PGNiG before hydraulic fracturing operations. Data was later on reprocessed bringing additional information after applying anisotropic prestack time migration and time frequency domain noise rejection (see Smolarski et al., 2014). The processed data was further analyzed with a dip steered semblance attribute. This attribute is a measure of similarity between waveforms of neighboring traces (Chopra and Marfurt, 2007) and is routinely used for fault interpretation. In this dataset it shows additional proof of fault presence at this location with a clear semblance anomaly in NNW – SSW direction (Fig. 6).

Figure 7 illustrates the similarity of the waveforms from two groups of events from Stage 1. Not only the events can be divided into two groups of highly similar waveforms, these two groups have nearly opposite phase of direct P- and S-waves. Figure 7 shows only Receiver 7 waveforms but the same similarity is observed for these events on all other components and receivers (Fig. 8). This means the events within each group have very similar P- and S-wave amplitudes and they originate from similar locations which imply very similar source mechanisms of events in each group. As the group has nearly opposite waveforms between the two groups the source mechanisms must be opposite in a sense of very similar dip and strike of their fault planes and reversed rake (see Cieplicki et al., 2012 for more details). The observed events from most of the stages can be separated into two groups of mutually opposite source mechanisms as is also observed by Rutledge et al. (2003) and Stanek and Eisner (2013).

DISCUSSION AND ACTIVE COMPARISON WITH ACTIVELY IMAGES

The observed asymmetric distribution of the event locations relative to the treatment well for Stage 5 probably results from the asymmetric hydraulic fracture. In this stimulation the fracture probably grew twice as long to the east then to the west, although this observation is based on the least certain back azimuth observation. While the monitoring well is placed closer to the eastern event the asymmetry is most likely not resulting from the monitoring asymmetry as if there were events on the western site with similar magnitude they would be detected. This asymmetry is potentially a cause of reduced production as the produced gas must flow longer path from the eastern part of the fracture. However, as such asymmetry is also commonly observed on the North American microseismic monitoring projects of economically producing wells, it is unlikely this is the main cause of the reduced production if at all. Additionally the observed asymmetry is convincingly only observed for the Stage 5, which probably was also affected by the asymmetric interaction with existing fault.

Maxwell et al. (2011), Refunjol et al. (2012) and others describe correlation between induced microseismicity and natural faults mapped with active seismic monitoring. Smolarski et al. (2014) reprocessed active seismic dataset acquired over this area. The dataset was acquired with vibroseis with relatively high nominal fold. It was necessary to use weak anisotropic parameters to optimally image the observed faults as discussed above. Two main faults were interpreted in SW-NE and SE-NW directions (Kowalski et al., 2014). However, there were no interpreted faults in the vicinity of the L2H well originally. In the reprocessed dataset of the reflection seismic a small fault trending in the NNW-SSE direction at the horizontal part of fractured well was found and is shown in Figure 6. This fault is consistent with the upward growth of the microseismic cloud on the Stages 2 and 3 and higher event count of the Stages close to this identified fault as was also observed by Yang and Zoback (2014).

CONCLUSIONS

High data quality and large number of located microseismic events proves that Polish Baltic Basin Silurian and Ordovician shale gas deposits can be stimulated with known hydraulic fracturing methods successfully and they respond to stimulations with similar microseismic activity as observed in the North American shale deposits.

The observed shear wave splitting of micro-seismic data shows that the Polish shale formations are anisotropic. The observed microseismicity indicates asymmetric growth of the hydraulic fracture

with preferential growth toward east. We also observe that microseismic events have two groups of highly similar events of mutually opposite source mechanisms. Both phenomena are commonly observed in the North American shale gas stimulations mapped by microseismic monitoring.

Generally induced seismicity stayed at the fractured intervals vertically with small number of microseismic events growing out of zone on two stages. This vertical growth of the microseismicity is observed where a small identified fault intersected the stimulated well indicating an activation of a pre-existing natural fault. This observation may explain low productivity from these stages as the gas is unlikely to flow downwards from the stimulated fault.

ACKNOWLEDGMENTS

This study was supported by the Grant of The Polish National Center for Research and Development in the Program Blue Gas, project entitled "Appraisal of microseismic monitoring techniques of hydraulic fracturing and development of optimal processing and interpretation methodologies" (Acronym: SHALEGASMICROS). Authors are thankful to PGNiG S.A. for providing the microseismic dataset. The research was also financed by the AGH-UST grants no. 15.11.140.872 and 15.11.140.870.

REFERENCES

Bardainne, T. and Gaucher, E.: 2010, Constrained tomography of realistic velocity models in microseismic monitoring using calibration shots. Geophysical Prospecting, 58, 1365–2478. DOI: 10.1111/j1365-2478.2010.00912.x

Chopra, S. and Marfurt, K.J.: 2007, Seismic attributes for prospect identification and reservoir characterization. Geophysical Developments Series, Society of Exploration Geophysics, 1. DOI: 10.1190/1.9781560801900

Cieplicki, R., Eisner, L. and Abbott, D.: 2012, Correlation, detection and location for microseismic events induced by hydraulic fracturing. 74th EAGE Conference and Exhibition incorporating EUROPEC 2012. DOI: 10.3997/2214-4609.20148208

Duncan, P. and Eisner, L.: 2010, Reservoir characterization using surface microseismic monitoring. Geophysics, 75, 75A139-75A146. DOI: 10.1190/1.3467760

Eisner, L., Bulsey, B., Duncan, P., Jurick, D., Werner, H. and Keller, W.: 2010, Comparison of surface and borehole locations of induced seismicity. Geophysical Prospecting, 58, 809–820. DOI: 10.1111/j1365-2478.2010.00867.x

Fischer, T., Hainzl, S., Eisner, L., Shapiro, S. and Le Calvez, J.: 2008, Microseismic signatures of hydraulic fracture growth in sediment formations: observations and modeling. Journal of Geophysical Research, 113, B02307. DOI: 10.1029/2007JB005070

Grechka, V., Singh, P. and Das, I.: 2011, Estimation of effective anisotropy simultaneously with locations of microseismic events. Geophysics, 76, WC141–WC155. DOI: 10.1190/geo2010-0409.1

Grechka, V., Theophanis, S. and Tsvankin, I.: 1999, Joint inversion of P- and PS-waves in orthorhombic media: Theory and a physical modeling study. Geophysics, 64, 146–161. DOI: 10.1190/1.1444512

Kowalski, H., Godlewski, P., Kobusinski, W., Makarewicz, J., Podolak, M., Nowicka, A., Mikolajewski, Z., Chase, D., Dafni, R., Canning, A. and Koren, Z.: 2014, Imagning and characterization of a shale reservoir onshore Poland, using full- azimuth seismic depth imaging. First Break, 32, 101–109. DOI: 10.3997/2214-4609.20141208

Maxwell, S., Bennett, L., Jones, M. and Walsh, J.: 2010, Anisotropic velocity modeling for microseismic processing: Part 1 – Impact of velocity model uncertainty. 80th Annual International Meeting, SEG, Expanded Abstracts, 2130–2134. DOI: 10.1190/1.3513267

Maxwell, S., Cho, D., Pope, T., Jones, M., Cipolla, C., Mack, M., Henry, F., Norton, M. and Leonard, J.: 2011, Enhanced reservoir characterization using hydraulic fracture microseismicicty. SPE Hydraulic Fracturing Technology Conference, 24-26 January, The Woodlands. DOI: 10.2118/140449-MS

Menanno, G., Vesnaver, A. and Jervis, M.: 2012, Borehole receiver orientation using a 3D velocity model. Geophysical Prospecting, 61, 215–230. DOI: 10.1111/j.1365-2478.2012.01106.x

Refunjol, X.E., Keranen, K.M., Calvez, J.H. and Marfurt, K.J.: 2012, Integration of hydraulically induced microseismic event locations with active seismic attributes: A North Texas Barnett Shale case study. Geophysics, 77, KS1–KS12. DOI: 10.1190/geo2011-0032.1

Ruttledge, J.T. and Phillips, W.S.: 2003, Hydraulic stimulation of natural fractures as revealed by induced microearthquakes, Carthage Cotton Valley gas field, east Texas. Geophysics, 68, 441–452. DOI: 10.1190/1.1567214

Smolarski, L., Mackowski, T. and Pasternacki, A.: 2014, Comparative analysis of seismic images 2D and 3D surveys in the area of Lubocino, Geopetrol – exploration and production of oil and natural gas reservoirs – new technologies, new challenges, Expanded Abstracts, 201–205.

Stanek, F. and Eisner, L.: 2013, New model explaining inverted source mechanisms of microseismic events induced by hydraulic fracturing. 83rd Annual International Meeting, SEG, Expanded Abstracts, 2201–2205. DOI: 10.1190/segam2013-0554.1

Yang, J and. Zoback, M.D.: 2014, The role of preexisting fractures and faults during multistage hydraulic fracturing in the Bakken Formation Interpretation. Geophysics, 2(3), SG25–SG39. DOI: 10.1190/INT-2013-0158.1

Warpinski, N., Sullivan, R., Uhl, J., Waltman, C. and Machovoe, S.: 2005, Improved microseismic fracture mapping using perforation timing measurements for velocity calibration. Society of Petroleum Engineers, 10, 14–23. DOI: 10.2118/84488-MS

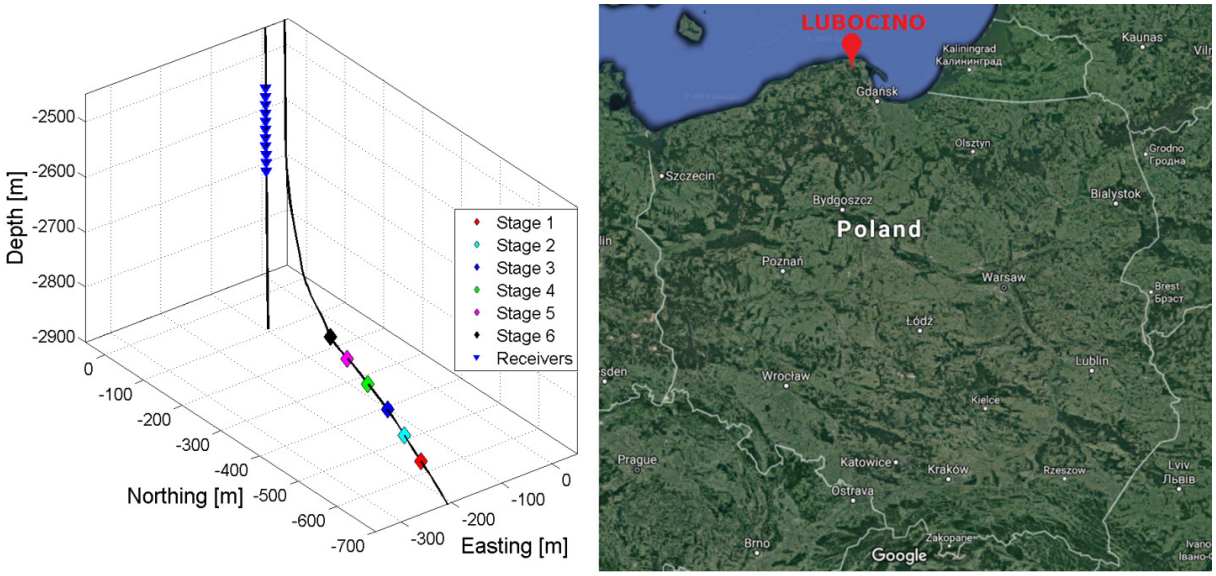

Fig. 1 Oblique view of the downhole microseismic array and the map view of the site. The microseismic array (blue triangles) in the nearly vertical well L1, and the treatment horizontal well L2H with six stages (colored diamonds). Stage 1 is shown with red diamond and the last Stage 6 is shown as black diamond.

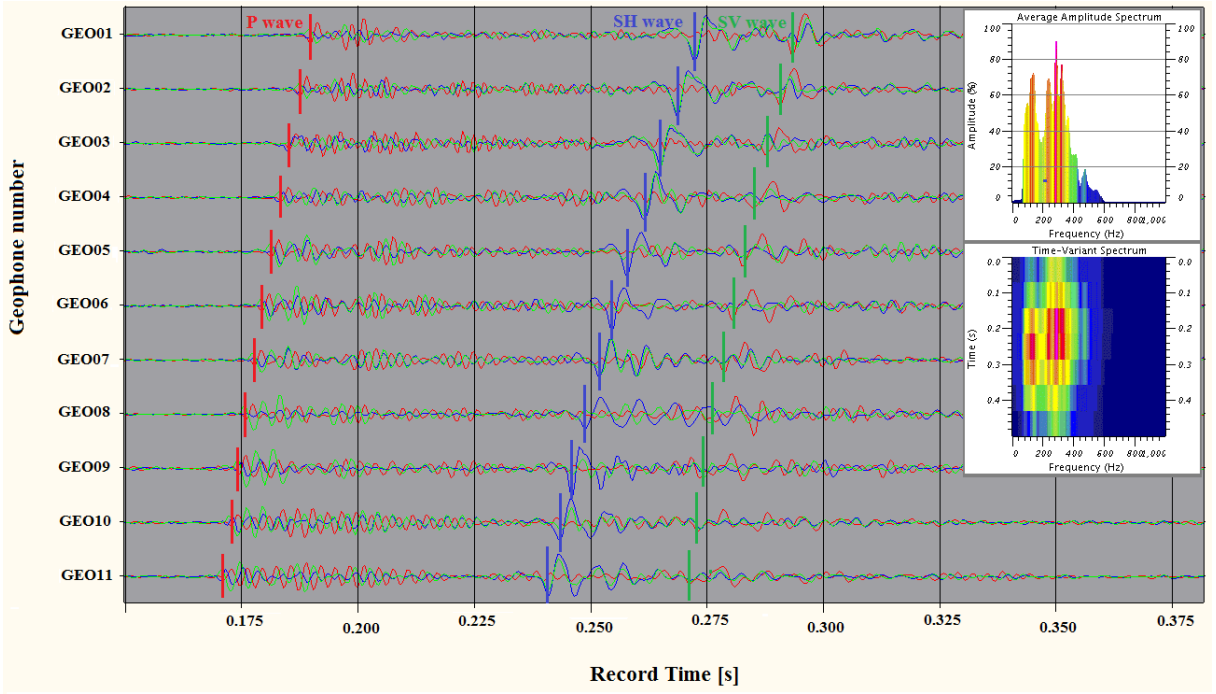

Fig. 2 Particle velocity seismograms with the arrival time picks of a typical microseismic event from stage 4. The thress components overlayed: Vertical component – red line, East component – blue line, North component – green line. Amplitude and spectrogram is shown in the two insets in the upper right corner. The amplitude spectrum is East component over the time interval shown in this Figure, the spectrogram represents East component of the time interval including both P and S-wave on GEO10 receiver.

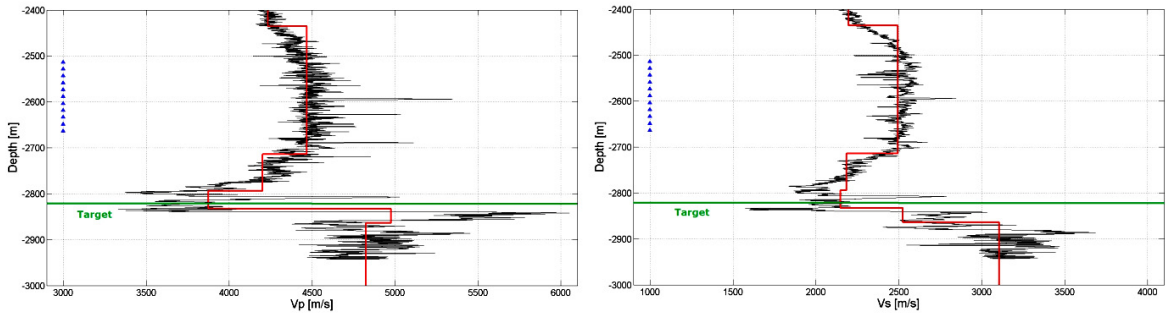

Fig. 3 Compressional and shear sonic logs (black) and layered velocity models (red) of the investigated area. The clue triangles represent depth of the monitoring receivers, green line is approximate depth of the stimulated well.

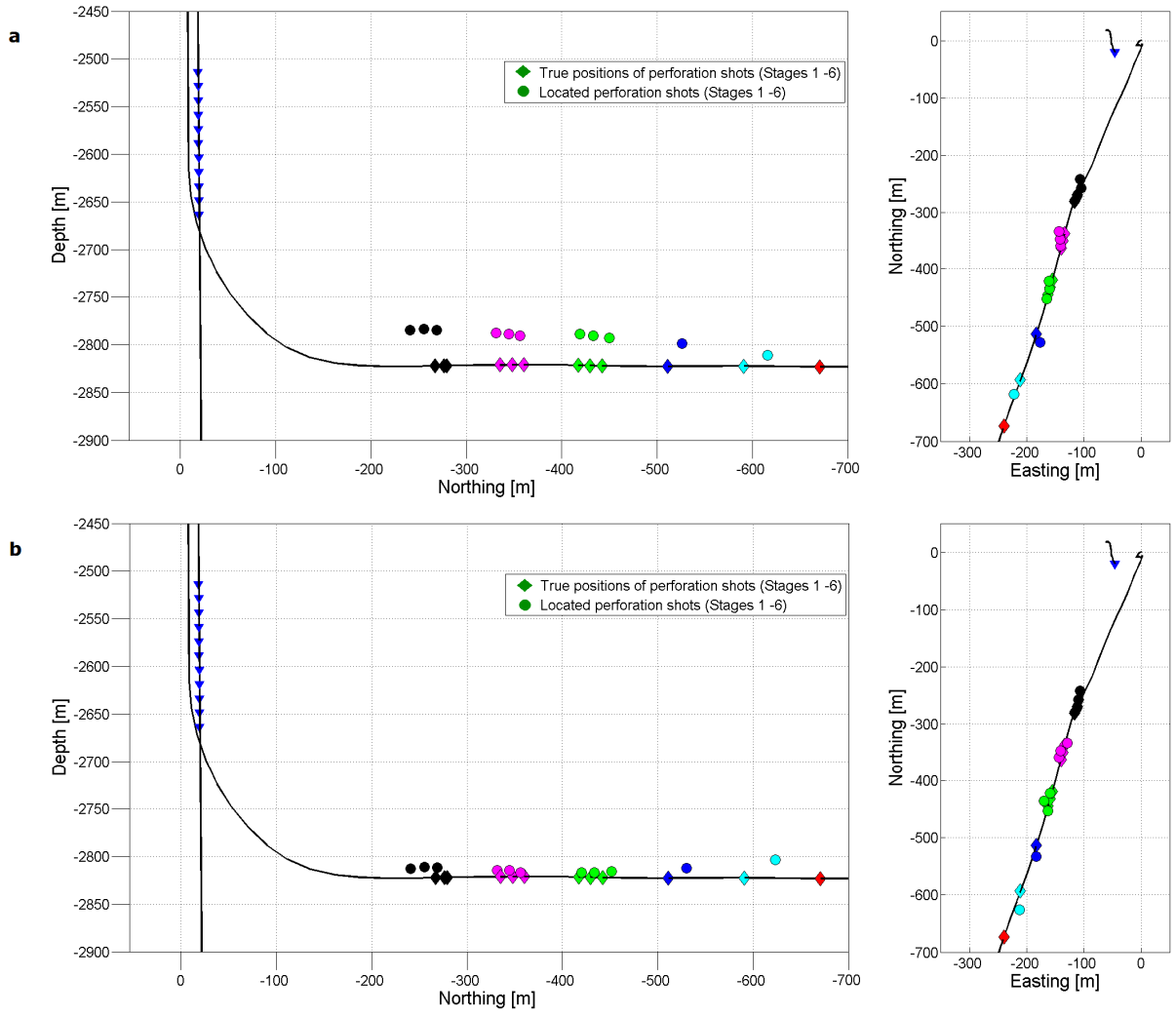

Fig. 4 Vertical cross-section (south-north) and map view of perforation shot locations (coloured dots) in isotropic (a) and calibrated anisotropic (b) velocity model. The true positions of perforation shots are represented by the colored diamonds as in Figure 1.

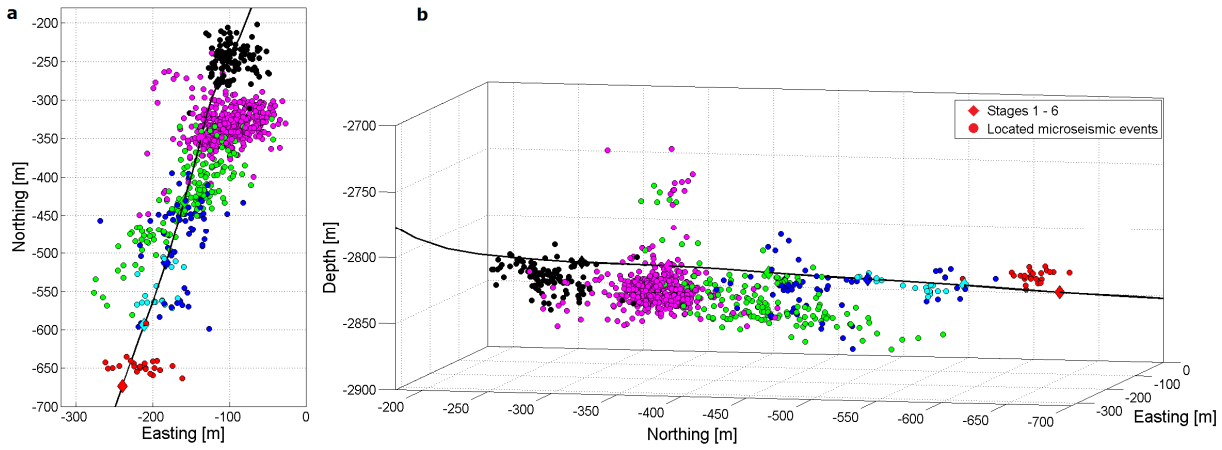

Fig. 5 Map view (a) and oblique view (b) of microseismic events located in the calibrated anisotropic velocity model. Events are colored by stages consistently with Figure 1. The true perforation intervals are shown as corresponding diamonds.

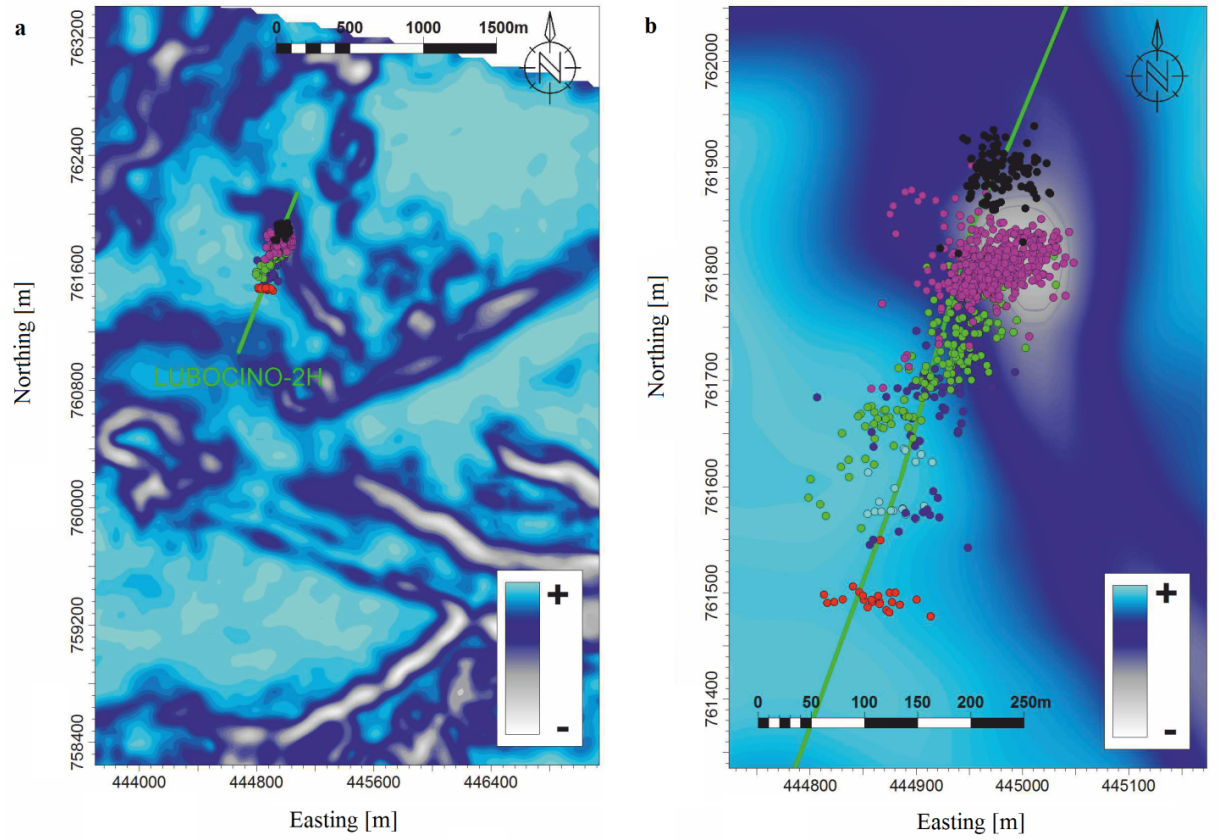

Fig. 6 Map view of the Semblance attribute of 3D migrated section of active seismic data over the area of the horizontal section of the well L2H (a) and its zoom (b) with the microseismic data overlaid in regional coordinate system. The grey area represents an area of low semblance representing potential NNE-SSW trending fault.

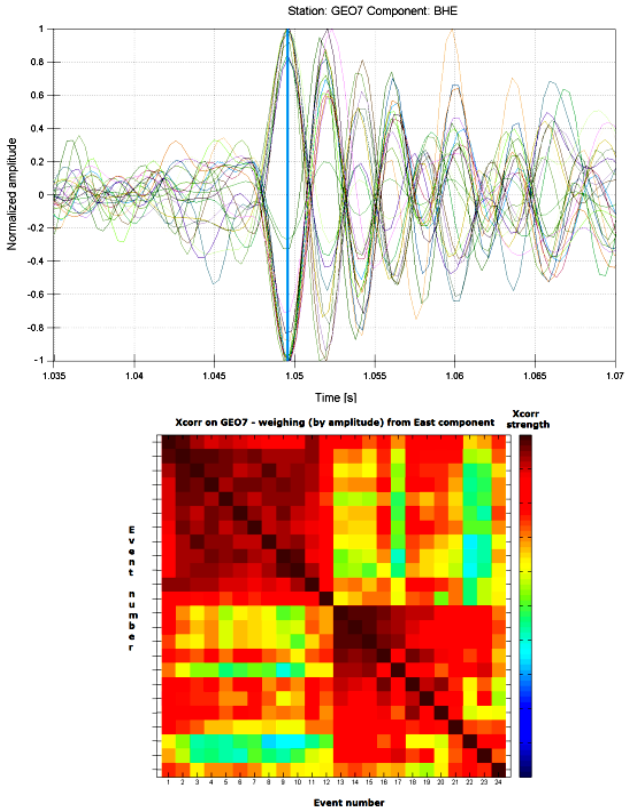

Fig. 7 Top plot: Particle velocity waveforms of events from the Stage 1 aligned on the S-wave arrival recorded on east component of the geophone 7 shown in Figure 1. The cyan vertical line represent the S-wave pick. No filtering was applied to data. Lower plot: cross-correlations of the waveforms above in the time interval shown in the plot above.

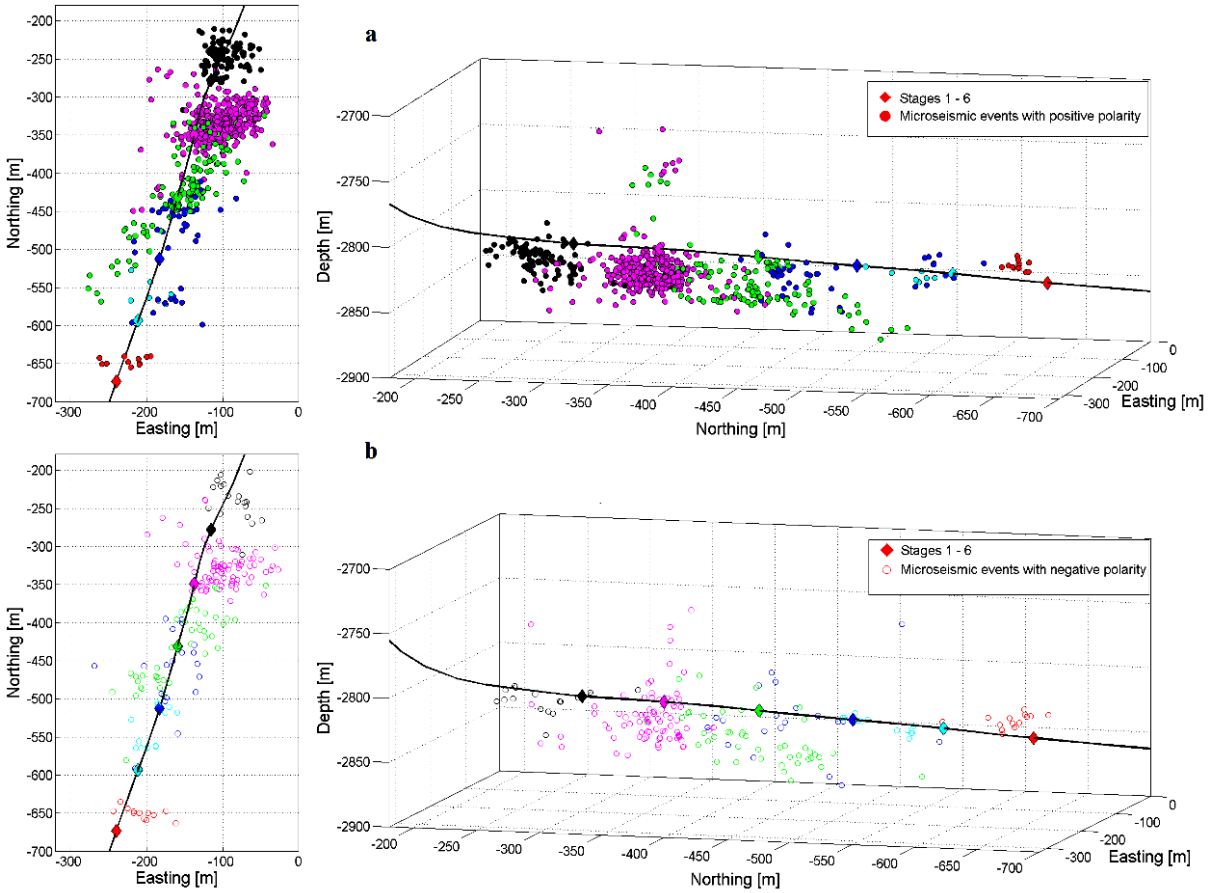

Fig. 8 Vertical cross-section and map view of microseismic events separated into two groups with opposite polarity located in the calibrated anisotropic velocity model. Events with positive polarity – full dots (a), events with negative polarity – empty dots(b). Events are colored by stages consistently with Figure 1. The true perforation intervals are shown as corresponding diamonds.